Scientific Research

Effect of Annealing on the Structural and Optical Properties of $CuIn_{1-x}Al_xS_2$ Thin Films

Fethi Smaili[*]

Laboratoire de Photovoltaïque et Matériaux Semi-conducteurs, Tunis, Tunisie.
Email: [*]smaili.fethi@gmail.com

ABSTRACT

The effects of annealing of $CuIn_{1-x}Al_xS_2$ thin films for different temperature, which were grown by thermal evaporation, were investigated through X-ray diffraction (XRD), energy dispersive X-ray analysis (EDS) and optical absorption measurements. Post growth was used to modify the structural and optical properties of the CIAS thin films. Then it realized in three different temperatures 250°C, 300°C and 400°C. It is found that significant difference of the transparent films in function of annealing temperature. The FWHM in the X-ray diffraction pattern is found to decrease with an increase in annealing temperature indicating that the crystalline nature of the CIAS improves with increase in annealing temperature. The position of the (112) peak and other peaks in the X-ray diffraction pattern has been observed to shift to higher values of 2θ with the increase of gallium concentration. We demonstrate a significant enhancement of the inter-diffusion in the dot thin film.

1. Introduction

Ternary and quaternary compound semiconductors of the type I-III-VI$_2$ have received much attention in recent years because of their potential application in optoelectronic devices [1]. Significant effort has been made to increase the band gap in order to improve the module performance, resulting from the trade-off between higher voltages and lower currents at maximum power. Conversion efficiencies for polycrystalline CIGS based solar cells have been significantly improved over recent years and the best cell is now reported at 19.5% [2]. However, among ternary chalcopyrite semiconductors, CuInS$_2$ may be the most promising material for photovoltaic applications due to the band gap energy of 1.53 eV [3]. In the search for a lattice matching between the absorbent layer and a window buffer layer, also the Ga is a scarce and expensive material and therefore it can be replaced by inexpensive abundant aluminium Al. Cu(In$_{1-x}$Al$_x$)S$_2$ [CIAS] has been considered as promising alternative, since it requires less aluminium concentration than gallium to achieve a similar band gap [4]. In addition to single junction solar cells, CIAS thin films can also find application in tandem solar cells [5,6].

Very little is understood about the formation of intrinsic defects in this material, and a detailed study of these defects and impurity levels relating to the composition of the material is necessary in order to fabricate devices [7]. CIAS thin films have been prepared by several techniques including co-evaporation [8,9], one step RF magnetron sputtering [10], chemical bath deposition (CBD) [11] and sequential deposition methods [12-14]. The various types of annealed films have a great effect on their structural, morphological and optical properties. The film characteristics depend on the methods and post-growth treatments conditions while high performance films were generally obtained with expensive techniques [15].

In this study, we report the effects of annealed in various temperatures on the structural, compositional and optical properties of CIAS films.

2. Experiments

2.1. Film Preparation

We prepared by vacuum thermal evaporation $CuIn_{1-x}Al_xS_2$ films by charging polycrystalline $CuIn_{1-x}Al_xS_2$ powders as source materials into heated tungsten crucibles. The base pressure during the evaporation was 10^{-6} Torr. The glass substrate temperature was kept at 200°C. Substrate heating was achieved by the heater system described elsewhere [16]. This system allowed us to insert a suit-

able Cu-based alloy cylinder with a diameter $d \leq D$, where D is the heater diameter ($D = 100$ mm), between the heater and the substrate holder. The cylinder thickness was kept constant (1 cm). The distance from crucible to sample holder was 10 cm. The substrate temperature was measured using a thermocouple in contact with the substrate surface. After deposition the samples were annealed in free different temperatures, in vacuum at 250˚C and 300˚C and under nitrogen atmosphere at 400˚C for 1 h. The thermal annealing was performed on sample pieces with an area of about 2 cm^2. The thin film was placed in a quartz tube. During the annealing process, a flow of nitrogen was passed through the tube.

2.2. Characterization of CuIn$_{1-x}$Al$_x$S$_2$ thin Films

Optical transmittance (Texp) and reflectance were measured at normal incidence in the wavelength range 300 - 1800 nm with an UV-visible-NIR Shimadzu 3100 S spectrophotometer equipped with an integrated sphere. The film's thicknesses were calculated from the positions of the interference maxima and minima of reflectance spectra using a standard method [17], the absorption coefficient was deduced [18]. The compositions of the films were determined by EDX measurement. Whereas the structural properties were determined by the X-ray diffraction technique using CuK radiation ($\lambda = 0.15418$ nm).

3. Results and Discussion

3.1. Structural Properties

Figure 1 shows the X-ray diffraction pattern of the annealed CuIn$_x$Al$_{1-x}$S$_2$ thin films of four different compositions and free different temperatures. From these patterns, it is observed that all the films are polycrystalline in nature. Peaks corresponding to metallic phase or binary sulfed/oxide phase are not observed. This indicates that the films are single phase. Then, for the annealing at 250˚C we can note a no improvement in crystallinity is observed and there is no difference from the not annealed CIAS thin films (not shown) due to the low temperature annealing, which seems inadequate for a possible improvement of the disappearance of copper phase.

In addition, we note a disappearance of minor peaks correspond with copper phase for the CIAS thin films annealed at 300˚C. But we note a complete disappearance of these peaks and an improvement of the crystallinity of the CIAS films, which presents small peaks (200), (220), (116) and (224) for the CuInS$_2$ phase. Indeed, the presence of small peaks indicates that the small grains were formed during annealing at temperatures higher than 300˚C.

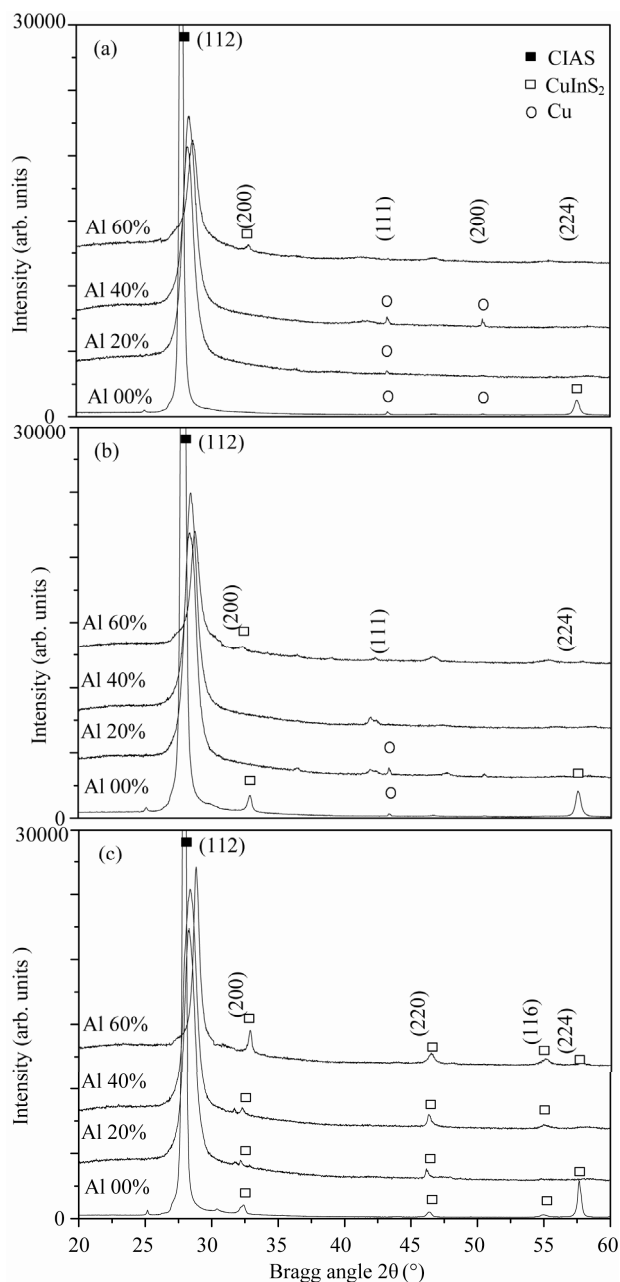It is clear that the annealing under nitrogen at 400˚C

Figure 1. X-ray diffraction patterns of annealed CuIn$_{1-x}$Al$_x$S$_2$ thin films for different composition and at various temperatures (a) 250˚C, (b) 300˚C and (c) 400˚C.

which is equivalent to a vacuum annealing greatly improves the crystallinity of the films.

The position of the peak corresponding to the (112) orientation is found to shift to higher values of 2θ. This noticeable shift of the main Bragg peak to large angles is due to the decrease in lattice constants "a" and "c" and therefore the "d" spacing. The shift of the diffraction peak to higher angle and the decrease of lattice parameter with increase of aluminium content in the studied compositions

are in accordance to Vegards law [1]. These results indicate that CIAS solid solution has been successfully obtained without any phase separation into CIS or CAS or any other secondary phases. We here with report and discuss the structural parameters of the CIAS thin films.

The lattice parameters for the CIAS thin films have been evaluated and are shown in **Table 1**. The lattice parameter values "a" and "c" are found to decrease as aluminium concentration increases. This may be due to the fact that aluminium atom is smaller in size than indium atom and hence causes shrinkage in the lattice as they substitute indium sites in the cell. The FWHM is found to increase as the aluminium concentration increases and this can be attributed to the incorporation of the aluminium element in the indium sites, which distorts the normal lattice structure of CuInS$_2$. The observed increase in FWHM values corresponds to a decrease in the effective grain size with increased aluminium incorporation into the network parameter of CuInS$_2$.

The average crystallite size can be calculated using the cherrer equation [19]:

$$D = \frac{0.9\lambda}{B\cos\theta} \quad (1)$$

where λ is the x-ray wavelength, θ is the Bragg diffraction angle, and B is the full-width at half-maximum (FWHM) of the peak corresponding to θ. When calculated by using the peak corresponding to the (112) plane of CIAS. **Figure 2** shows that the average grain size is found to decrease as well as aluminium concentration increase (**Table 1**).

3.2. Compositional Analysis

The chemical constituents present in the thin films have been identified using energy dispersive X-ray analysis. The composition of the CIAS thin films are shown in **Table 2**. The composition of the CIAS films were tested at four different regions on the film surface and the values reported in **Table 2** are an average of the atomic percentage of each element. As can be seen in **Table 1**,

Table 1. Structural parameters of CIAS films.

Samples		Lattice parameter			Film thickness (nm)	FWHM	Grain size (Å)
		a (Å)	c (Å)	d_{112} (Å)			
Annealed at 250˚C	CIAS: Al 00at.%	5.524	11.159	3.1997	480	0.247	320
	CIAS: Al 20at.%	5.503	10.723	3.1491	320	0.986	79
	CIAS: Al 40at.%	5.496	10.632	3.1375	310	0.992	75
	CIAS: Al 60at.%	5.474	10.421	3.1073	300	0.8232	76
Annealed at 300˚C	CIAS: Al 00at.%	5.524	11.159	3.1997	440	0.236	340
	CIAS: Al 20at.%	5.498	10.712	3.1461	450	0.937	86
	CIAS: Al 40at.%	5.492	10.633	3.1361	350	0.982	77
	CIAS: Al 60at.%	5.480	10.348	3.1017	380	0.687	89
Annealed at 400˚C	CIAS: Al 00at.%	5.524	11.109	3.1949	490	0.177	390
	CIAS: Al 20at.%	5.502	10.771	3.1534	460	0.922	92
	CIAS: Al 40at.%	5.497	10.686	3.1433	400	0.998	90
	CIAS: Al 60at.%	5.473	10.333	3.0974	460	0.510	102

Table 2. Thin films elemental compositions (at.%).

Samples		S	In	Cu	Al	O	$\frac{Cu}{In+Al}$	$\frac{Al}{In+Al}$	$\frac{S}{Cu+In+Al}$	E_g
Annealed at 250˚C	CIAS: Al 00at.%	49.91	24.86	25.22	--	0	1.01	0.00	1.00	1.47
	CIAS: Al 20at.%	49.38	20.06	25.15	4.85	0.11	1.00	0.19	0.99	1.50
	CIAS: Al 40at.%	50.03	16.17	24.36	9.73	0.13	0.96	0.38	1.00	1.68
	CIAS: Al 60at.%	49.26	11.05	25.36	14.14	0.15	0.95	0.56	0.97	1.98
Annealed at 300˚C	CIAS: Al 00at.%	50.03	25.17	24.76	--	0	0.98	0.00	1.00	1.43
	CIAS: Al 20at.%	49.91	19.96	25.02	5.15	0.12	1.00	0.21	1.00	1.54
	CIAS: Al 40at.%	49.56	15.25	25.26	10.04	0.13	1.00	0.40	0.98	1.81
	CIAS: Al 60at.%	50.03	10.57	24.36	15.13	0.15	0.99	0.59	1.00	1.84
Annealed at 400˚C	CIAS: Al 00at.%	48.91	24.86	26.22	--	0	1.05	0.00	0.96	1.45
	CIAS: Al 20at.%	49.26	19.25	26.36	5.04	0.14	1.09	0.21	0.97	1.50
	CIAS: Al 40at.%	48.93	15.67	25.96	9.43	0.15	1.03	0.38	0.96	1.60
	CIAS: Al 60at.%	49.06	9.54	26.16	16.04	0.17	1.02	0.63	0.95	1.85

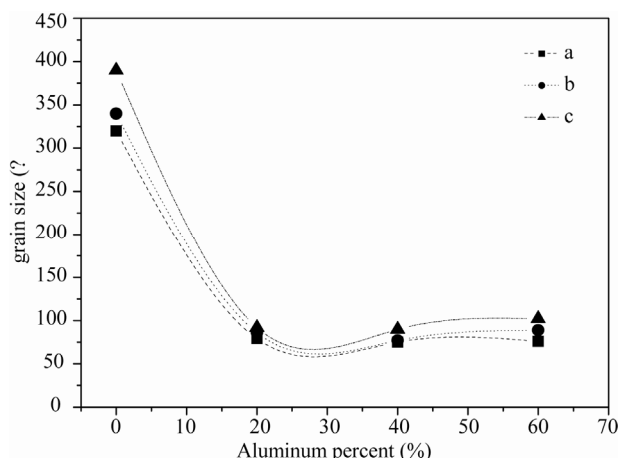**Figure 2. Grain sizes of CuIn$_{1-x}$Al$_x$S$_2$ thin films versus aluminum content percent for various temperatures (a) 250˚C, (b) 300˚C and (c) 400˚C.**

the ratio of Cu, In, Al and S elements in the CIAS film is almost 1: 1: 2.

It is seen that the ratio of Cu/(In + Al) is near of the unity and the ratio of S/(Cu + In + Al) is close to unity. In addition, we note an increase in the Al/(In + Al) ratio from 0 to 0.59 which is almost the composition of the used powders.

3.3. Optical Properties

3.3.1. Transmission and Reflection Spectra

The optical transmission curves of CIAS thin films for different annealing temperatures are depicted respectively in **Figure 3** and **Figure 4**. The samples showed a semitransparent behaviour in the infrared region and the thinnest and lowest Al content CIAS sample presented also a relatively high transmission in the visible spectrum. The transmission spectrums of the CuInS$_2$ thin film show interference pattern with sharp fall of transmittance at the band edge for different annealing temperatures, which is an indication of good crystallinity. However, the transmissions of other films decrease strongly when the aluminium percent increase in the materials; this is probably due to the inhomogeneities of the films.

In addition, we note a decrease in the transmission values for the CIAS thin films annealed at 250˚C and 300˚C for about 10% and 30% respectively. We explain this decrease after annealing by the substitution of the indium element by the aluminium and the diffused aluminium from the surface into the volume.

Figure 3(c) shows the optical transmission spectra of CIAS films annealed at 400˚C. For CuInS$_2$ film, we point out the presence of the interference fringes due to the multitude reflection phenomena showing homogenous films. Moreover these films exhibit a good transparency
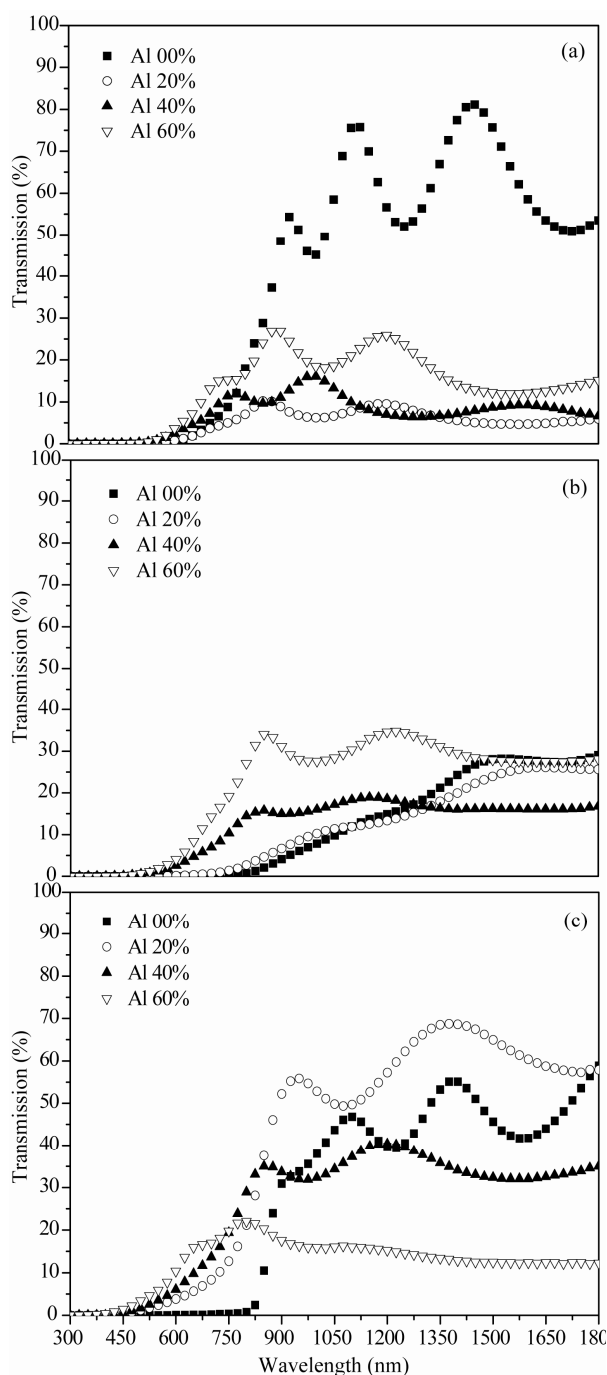

Figure 3. Transmission spectra of annealed CuIn$_{1-x}$Al$_x$S$_2$ thin films for different composition and at various temperatures (a) 250˚C, (b) 300˚C and (c) 400˚C.

in the visible and infrared regions. Than these interferences disappear when we increase the aluminium content in the CIAS thin films and the transmission values decrease as a function of the aluminium percent and varies from 70% to 10%, this is probably due to the inhomogeneities present in the volume and the perturbed relief on
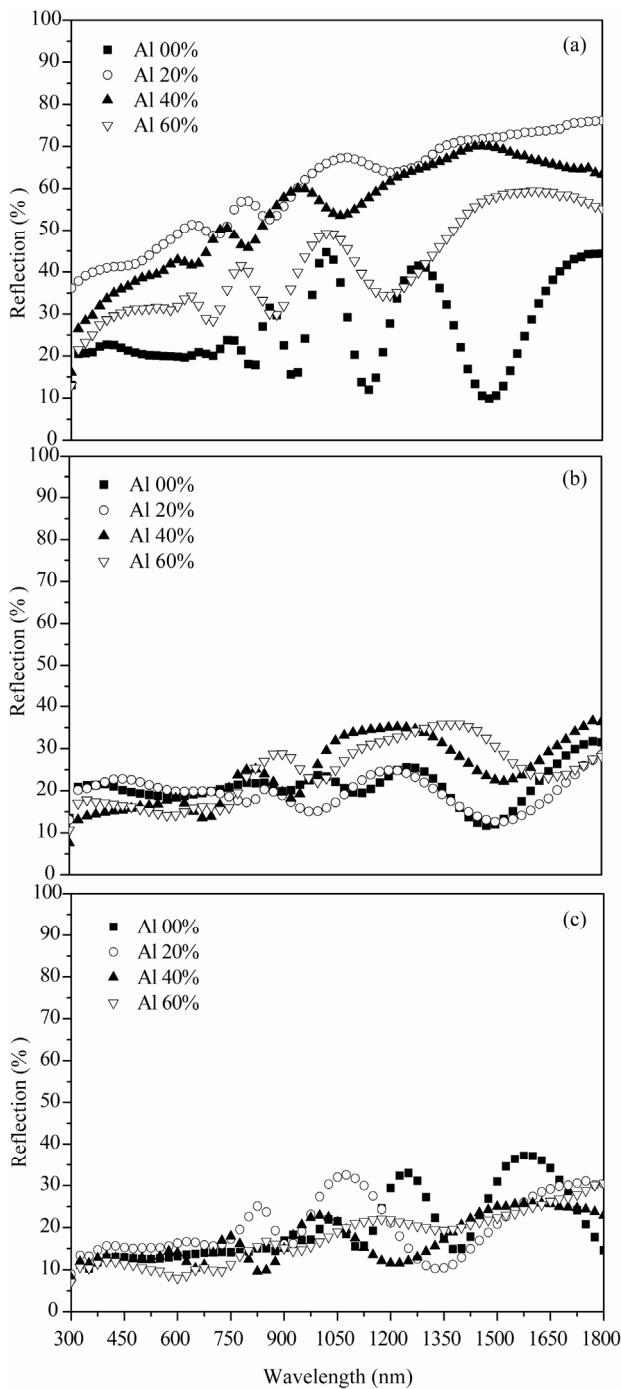
Figure 4. Reflection spectra of annealed CuIn$_{1-x}$Al$_x$S$_2$ thin films for different composition and at various temperatures (a) 250˚C, (b) 300˚C and (c) 400˚C.

the surface.

Figure 4(a) shows the optical reflection spectra of CIAS films annealed at 400˚C. We notice an increase in the reflection values for the CIAS films for about 70% compared to the non alloyed films. The reason of the

increase of the reflection is that the aluminium is localized near the surface rather than in the volume. Indeed, after annealing at 300˚C and 400˚C one can note a decrease of the reflection values from 70% to 25% and an improvement decrease of the interference fringes (**Figure 4(c)**). We explain these phenomenons by the diffusion of aluminium from the surface into the volume and an indication of poor crystallinity.

3.3.2. Absorption Coefficients

The absorption coefficient has been calculated using Equation (2) [20,21] and by means of optical transmission and reflection data taken at 300 K:

$$\alpha = \frac{1}{d} Ln\left(\frac{(1-R)}{T}\right) \qquad (2)$$

where α is the absorption coefficient, d is the thickness of the film, T and R are the transmission and reflectance, respectively. **Figure 5** shows the absorption coefficients as a function of the photon energy for CIAS thin films. The main absorption appears in the high photon energy region between 10^4 cm^{-1} and 10^5 cm^{-1} in the visible and the near-IR spectral range. But additional absorption features are found in the low energy range from 1.5 to 3 eV. This suggests that band-to-band optical transitions occur in the high photon energy region (hv > 2 eV), while, on the other hand, transitions between the ionized donor and the conduction band appear in the lower energy region. The presence of a single absorption edge is explained by the disappearance of secondary phases such as Cu, a result confirmed by X-ray diffraction analysis of annealing temperatures are above 300˚C. It is observed that there is dependence between the absorption value and the composition of the films. Then the incorporation of aluminium atoms moves the absorption coefficients on the left, we assume that are easily diffused in the volume during annealing process. This result is very important since the spectral dependence of the absorption coefficient affects the solar conversion efficiency [22]. The absorption coefficient α is related to the energy gap E_g according to the equation:

$$\alpha(hv) = A\left(hv - E_g\right)^n \big/ hv \qquad (3)$$

where A is a constant, h is the Planck constant and n equal to 1/2 for direct gap and 2 for an indirect gap. Based on the allowed direct inter-band transition, the band-gap E_g was determined by extrapolating the straight line of the $(\alpha hv)^2$ vs. hv curve to intercept of the horizontal photon energy axis. The band gap energy increases with increasing the composition ratio for different annealing temperatures (**Table 2**). Probably, the increase of E_g may be attributed to the enhancement of
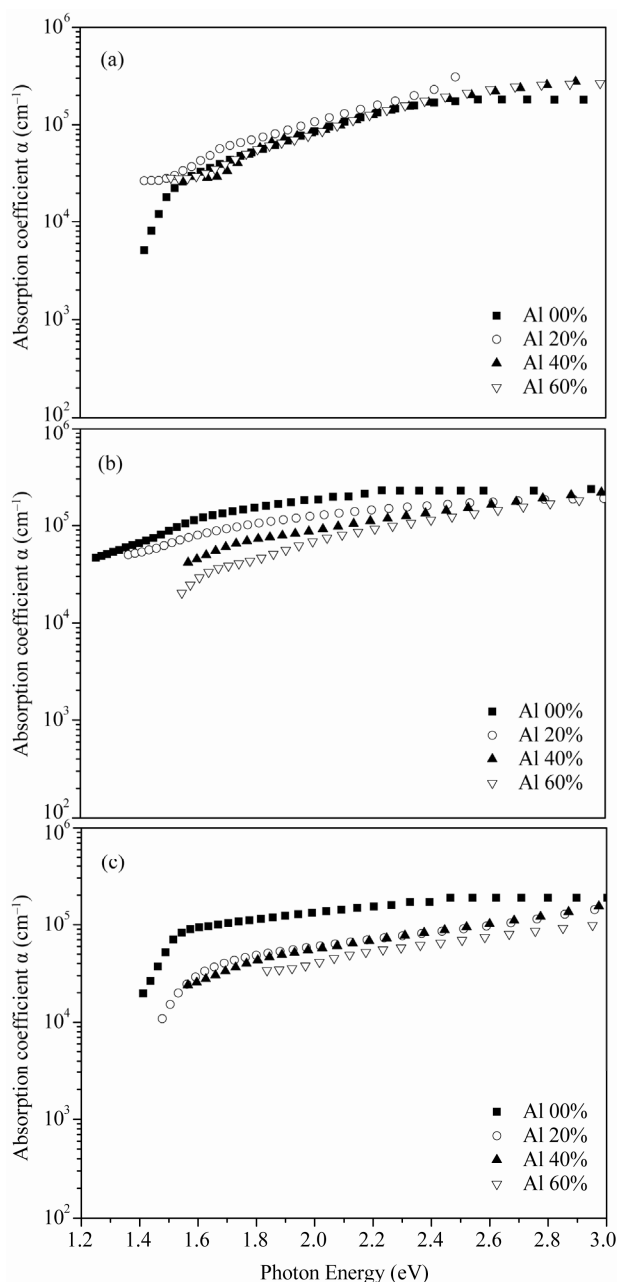
Figure 5. *α* **versus the photon energy (*hv*) of annealed CuIn$_{1-x}$Al$_x$S$_2$ thin films for different composition and at various temperatures (a) 250°C, (b) 300°C and (c) 400°C.**

grain size and the increase of defects in microstructure (such as sulfur vacancies and atom displacements) and/or deviations from stoichiometry in the films, which give rise to defect states and thus induce smearing of absorption edge.

4. Conclusions

CIAS thin films were deposited on corning glass (7059) substrates from CuIn$_{1-x}$Al$_x$S$_2$ powders by vacuum evapo-

ration and annealed in different temperatures and techniques. X-ray diffraction analysis had shown preferred (112) orientation and its found to shift to higher values of 2θ. Than for chemical composition we note an increase in the Al/(In + Al) ratio from 0 to 0.59 which is almost the composition of the used powders. In addition for the optical properties we note that 400°C is the best degree of annealing temperature to obtain a material with a single absorption edge. Also it is found that this absorption edge shifts to higher photon energy with increasing Al concentration.

REFERENCES

[1] M. Venkatachalam, M. D. Kannan, S. Jayakumar, R. Balasundaraprabhu and N. Muthukumarasamy, "Effect of Annealing on the Structural Properties of Electron Beam Deposited CIGS Thin Films," *Thin Solid Films*, Vol. 516, No. 20, 2008, pp. 6848-6852. doi:10.1016/j.tsf.2007.12.127

[2] K. Ramanathan, G. Teeter, J. C. Keane and R. Noufi, "High Performance CIGS Thin Film Solar Cells: A Laboratory Perspective," 2005 *DOE Solar Energy Technologies Program Review Meeting*, Denver, 7-10 November 2005. doi:10.1016/j.tsf.2004.11.050

[3] J. L. Shay, B. Tell, H. M. Kasper and M. Schiavone, "*p-d* Hybridization of the Valence Bands of I-III-VI$_2$ Compounds," *Physical Review B*, Vol. 5, No. 12, 1972, pp. 5003-5005. doi:10.1103/PhysRevB.5.5003

[4] M. W. Haimbodi, E. Gourmelon, P. D. Paulson, R. W. Birkmire and W. N. Shafarman, "Cu(InAl)Se$_2$ Thin Films and Devices Deposited by Multisource Evaporation [Solar Cells]," *Proceedings of the* 28*th IEE Photovoltaic Specialists Conference*, Anchorage, Alaska, 2000, p. 454.

[5] T. J. Coutts, K. A. Emery and J. S. Ward, "Modeled Performance of Polycrystalline Thin-Film Tandem Solar Cells," *Progress in Photovoltaics*: *Research and Applications*, Vol. 10, No. 3, 2002, pp. 195-203.

[6] A. J. De Vos, "Detailed Balance Limit of the Efficiency of Tandem Solar Cells," *Journal of Physics D*: *Applied Physics*, Vol. 13, No. 5, 1980, pp. 839-846.

[7] M. S. Branch, P. R. Berndt, J. R. Botha, A. W. R. Leitch and J. Weber, "Structure and morphology of CuGaS2 thin films," *Thin Solid Films*, Vol. 431-432, 2003, pp. 94-98.

[8] S. Marsillac, P. D. Paulson, M. W. Haimbodi, R. W. Birkmire and W. N. Shafarman, "Transparent Oxide Optoelectronics," *Applied Physics Letters*, Vol. 81, No. 7, 2002, p. 1350. doi:10.1063/1.1499990

[9] Y. B. K. Reddy, V. S. Raja and B. Sreedhar, "Growth and Characterization of CuIn$_{1-x}$Al$_x$Se$_2$ Thin Films Deposited by Co-evaporation," *Journal of Physics D*: *Applied Physics*, Vol. 39, No. 24, 2006, p. 5124. doi:10.1088/0022-3727/39/24/005

[10] B. Munir, R. A. Wibowo, E. S. Lee and K. H. Kim, "One Step Deposition of Cu(In$_{1-x}$Al$_x$)Se$_2$ Thin Films by RF Magnetron Sputtering," *Journal of Ceramic Processing*

Research, Vol. 8, No. 4, 2007, p. 252.

[11] B. Kavitha and M. Dhanam, "In and Al Composition in Nano-Cu(InAl)Se$_2$ Thin Films from XRD and Transmittance Spectra," *Materials Science and Engineering B*, Vol. 140, No. 1-2, 2007, pp. 59-63. doi:10.1016/j.mseb.2007.03.011

[12] F. Itoh, O. Saitoh, M. Kita, H. Nagamori and H. Oike, "Growth and Characterization of Cu(InA1)Se$_2$ by Vacuum Evaporation," *Solar Energy Materials & Solar Cells-Solar Energy*, Vol. 50, No. 1-4, 1998, pp. 119-125. doi:10.1016/S0927-0248(97)00132-3

[13] E. Halgand, J. C. Bernède, S. Marsillac and J. Kessler, "Physico-Chemical Characterisation of Cu(In,Al)Se$_2$ Thin Film for Solar Cells Obtained by a Selenisation Process," *Thin Solid Films*, Vol. 480-481, 2005, pp. 443446. doi:10.1016/j.tsf.2004.11.039

[14] S. Jost, F. Hergert, R. Hock, M. Purwins and R. Enderle, "Real-Time Investigations of Selenization Reactions in the System Cu-In-Al-Se," *Physica Status Solidi A*, Vol. 203, No. 11, 2006, pp. 2581-2587.

[15] R. Brini, M. Kanzari, B. Rezig and J. Werckmann, "Effect of Annealing on Properties of CuInS$_2$ Thin Films," *European Physical Journal—Applied Physics*, Vol. 30, No. 3, 2005, pp. 153-158. doi:10.1051/epjap:2005031

[16] F. Chaffar Akkari, R. Brini, M. Kanzari and B. Rezig, "High Absorbing CuInS$_2$ Thin Films Growing by Oblique Angle Incidence Deposition in Presence of Thermal Gradient," *Journal of Materials Science*, Vol. 40, 2005, pp.

1-5.

[17] J. Tauc, "Optical Properties of Solids," North-Holland, Publ., Amsterdam, 1973, p. 277.

[18] M. Ben Rabeh, M. Zribi, M. Kanzari and B. Rezig, "Structural and Optical Characterization of Sn Incorporation in CuInS$_2$ Thin Films Grown by Vacuum Evaporation Method," *Materials Letters*, Vol. 59, No. 24-25, 2005, pp. 3164-3168. doi:10.1016/j.matlet.2005.05.045

[19] H. P. Klug and L. E. Alexander, "X-Ray Diffraction Procedure for Polycrystalline and Amorphous Materials," Wiley, New York, 1974.

[20] D. E. Milovzorov, A. M. Ali, T. Inokuma, Y. Kurata, T. Suzuki and S. Hasegawa, "Optical Properties of Silicon Nanocrystallites in Polycrystalline Silicon Films Prepared at Low Temperature by Plasma-Enhanced Chemical Vapor Deposition," *Thin Solid Films*, Vol. 382, No. 1-2, 2001, pp. 47-55. doi:10.1016/S0040-6090(00)01208-6

[21] T. M. Wang, S. K. Zheng, W. C. Hao and C. Wang, "Studies on Photocatalytic Activity and Transmittance Spectra of TiO$_2$ Thin Films Prepared by r.f. Magnetron Sputtering Method," *Surface and Coatings Technology*, Vol. 155, No. 2-3, 2002, pp. 141-145.

[22] V. V. Kindyak, V. F. Gremenonok, I. V. Bodnar, V. Rud Yu and G. A. Madvedkin, "Optical Properties of Laser-Evaporated CuGaSe$_2$ Films near and above the Fundamental Absorption Edge," *Thin Solid Films*, Vol. 250, No. 1-2, 1994, pp. 33-36. doi:10.1016/0040-6090(94)90160-0